Faraday
Discussions

Accepted Manuscript

**Faraday
Discussions**

**Royal Society of
Chemistry**

ROYAL SOCIETY
OF CHEMISTRY

ROYAL SOCIETY
OF **CHEMISTRY**

www.rsc.org/faraday_d

Nanocrystal Superlattices that Exhibit Improved Order On Heating: An Example of Inverse Melting?

5 **Yixuan Yu,[a] Avni Jain,[a] Adrien Guillaussier,[a] Vikas Reddy Voggu,[a] Thomas M. Truskett,[a] Detlef-M. Smilgies,[b] and Brian A. Korgel[*a]**

[a] *McKetta Department of Chemical Engineering, Texas Materials Institute, Center for Nano- and Molecular Science and Technology, The University of Texas at Austin, Austin, TX 78712-1062,*
10 *USA; E-mail: korgel@che.utexas.edu*
[b] *Cornell High Energy Synchrotron Source (CHESS), Cornell University, Ithaca, NY4853, USA.*

Grazing incidence small angle X-ray scattering (GISAXS) measurements
15 reveal that superlattices of 1.7 nm diameter, gold (Au) nanocrystals capped with octadecanethiol become significantly more ordered when heated to modest temperatures (50-60°C). This enhancement in order is reversible and the superlattice returns to its initially disordered structure when cooled back to room temperature. Disorder-order transition temperatures were
20 estimated from the GISAXS data using the Hansen-Verlet criterion. Differential scanning calorimetry (DSC) measurements of the superlattices exhibited exotherms (associated with disordering during cooling) and endotherms (associated with ordering during heating) near the transition temperatures. The superlattice transition temperatures also correspond
25 approximately to the melting and solidification points of octadecanethiol. Therefore, it appears that a change in capping ligand packing that occurs upon ligand melting underlies the structural transition of the superlattices. We liken the heat-induced ordering of the superlattices to an inverse melting transition.

30 ## 1 Introduction

Beginning with the seminal report of Brust, Schiffrin, and coworkers in 1994,[1] alkanethiol-capped gold (Au) nanocrystals have served as useful models for understanding the synthesis and assembly of organic ligand-stabilized nanocrystals. They are easy to obtain and use: the synthesis is typically carried out at room
35 temperature in air, requiring only a few mixing and separation steps; the nanocrystals are relatively stable and readily dispersible in non-polar solvents; and size distributions can be quite narrow.[2] With uniform particles, superlattices can be formed without difficulty; for example, simple drop-casting on a substrate[3] or liquid interface[4,5] can yield superlattices with relatively long-range order, and their
40 assemblies have been extensively studied.[6] Alkanethiol-capped Au nanocrystals tend to order with either face-centered cubic (fcc) or body-centered cubic (bcc) structures, depending on the nanocrystal size and the ratio of the ligand length to the core diameter.[3] The packing structure (i.e., fcc or bcc) can be relatively insensitive

to the assembly approach; however, the morphology of the assembly, the range of order, and nature of the superlattice defects, all depend on details like the nanocrystal concentration,[7] rate of solvent evaporation,[8,9] solvent-substrate interactions,[10] humidity,[11] the presence of excess ligand,[5,12] and even subtle differences in solvent polarity.[13-15] Alkanethiol-capped Au nanocrystals have provided a practical, yet perhaps deceptively simple, model for the study of colloidal particle self-assembly.

Ligand-stabilized nanocrystals are not simple *hard spheres* like the many of the typical sub-micrometer colloidal particles used in the past to mimic the behavior of condensed matter in its various states;[16-21] the soft organic ligand shell provides a buffer between particles even without the presence of solvent, creating a deformable "bond" that is sensitive to changes in temperature.[22,23] The interparticle interactions can be fitted to a Lennard-Jones potential.[24] Luedtke and Landman predicted in 1996 that it might be possible for assemblies of alkanethiol-capped Au nanocrystals to undergo phase transitions, such as superlattice melting.[25] To date, however, there have been no *reversible* structural transformations observed for alkanethiol-capped Au nanocrystal superlattices. The problem is that these nanocrystals are relatively prone to coalescence with only modest increases in temperature. For instance, dodecanethiol-capped Au nanocrystals have been observed to ripen and increase in size in superlattices heated to only $130^{o}C$ and then sinter at $190{\sim}200^{o}C$—well below the melting temperature of Au.[26] To date, the only reversible structure transitions in assemblies of any type of ligand-stabilized nanocrystals have been observed at modest temperatures. Hanrath and colleagues for example used room temperature solvent vapor annealing of PbSe nanocrystal superlattices to observe rearrangements between bcc, fcc and amorphous structures.[27-29] Under those conditions, ligand attachment to the nanocrystals remains intact and the interparticle interactions could be reversibly tuned.

Here, we finally show an example of a reversible structure transition in an assembly of alkanethiol-capped Au nanocrystals. A collection of somewhat polydisperse and small (1.67 ± 0.30 nm diameter) octadecanethiol-capped Au nanocrystals were studied by grazing incidence small angle X-ray scattering (GISAXS) with *in situ* heating. At room temperature, the assembly exhibits some body-centered cubic (bcc) superlattice structure, but is predominantly amorphous. Raising the temperature above $45\text{-}55^{o}C$ led to a well-ordered bcc superlattice. The ordering is reversible and the structure again disorders when returned to room temperature. Differential scanning calorimetry (DSC) exhibited an endotherm at the ordering transition during heating and an exotherm upon disordering during cooling. Ordering of the superlattice upon heating is akin to *inverse melting*, which has been observed in ${}^{3}He$,[30] and polymers, poly-4-methyl-pentene-1,[31] and syndiotactic polystyrene,[32] in which crystallization occurs upon heating and melting upon cooling.[33,34] In the case of the octadecanethiol-capped Au nanocrystals, the space-filling of the ligands appears to underlie the structural transition of the nanocrystal superlattice, as the transition temperatures correspond approximately to the melting and solidification temperatures of octadecanethiol.

2 Experimental Details

2.1 Materials

Gold (III) chloride trihydrate ($HAuCl_4 \cdot 3H_2O$, >99.9%), tetraoctylammonium bromide (TOAB, 98%), 1-dodecanthiol (>98%), 1-octadecanethiol (98%), sodium borohydride ($NaBH_4$,>98%) were purchased from Sigma-Aldrich. Toluene (99.9%) and absolute ethanol were purchased from Fisher. Deionized (DI) water was
5 obtained using a Barnstead Nanopure Filtration System.

2.2 Gold Nanocrystals

Au nanocrystals were synthesized with octadecanethiol capping ligands using a modified Brust-Schiffrin method.[1,35] In a typical synthesis, 10 mL of an aqueous
10 solution of 164 mg of $HAuCl_4 \cdot 3H_2O$ (0.415 mmol) is combined with a solution of 3.281 g of TOAB (6.0 mmol) in 40 mL of toluene and stirred for 1 hr. The aqueous phase is then discarded and 1-octadecanethiol (358.2 mg, 1.25 mmol) is added to the toluene solution. An aqueous solution of the reducing agent is made in an ice bath with 189 mg of $NaBH_4$ (5.0 mmol) in 10 mL of DI-H_2O. The $NaBH_4$ solution is
15 then combined with the toluene solution under stirring. After 12 hr, the organic phase is collected.

The nanocrystals were purified by antisolvent precipitation using volumetric ratios of 5:1 ethanol:toluene. Nanocrystals are collected between each precipitation step by centrifugation. After three washes, the nanocrystals were dispersed in 3 mL
20 of toluene and centrifuged to precipitate poorly capped nanocrystals from the sample. The nanocrystal size distribution was further narrowed by size selective precipitation using toluene/ethanol as the solvent/antisolvent pair.[36]

2.3 Solution and Grazing Incidence Small Angle X-ray Scattering (SAXS and GISAXS)

25 SAXS and GISAXS measurements were performed on D1 beam line of the Cornell High Energy Synchrotron Source (CHESS), using monochromatic X-ray radiation with a wavelength of 1.155 Å and bandwidth of ~0.017 Å. GISAXS and SAXS pattern images were acquired with a fiber coupled CCD camera (MedOptics) having 1024×1024 pixels with size of 46.9 μm × 46.9 μm and dynamic range of 14-bit for
30 each pixel. All patterns were dark current corrected, distortion corrected, and flat field corrected by the acquisition software with a sample-to-detector distance of 562.0 mm determined using silver behenate powder as a calibration standard.

Solution SAXS measurements were made with the X-ray beam incident angle at 0° using exposure times of 30 sec. Ten patterns were recorded and averaged by the
35 acquisition software. Measurements were made with Au nanocrystals dispersed in toluene at a concentration of 5 mg/mL in glass capillary tubes (1.2 mm diameter) horizontally secured on the top of stage. Background scattering of pure toluene and the capillary tube was subtracted prior to data fitting.

GISAXS data were recorded with an X-ray beam incident angle of 0.25^o and an
40 exposure time of around 0.01 to 0.5 sec. Nanocrystal assemblies were prepared by drop-casting 20 μL of toluene dispersion of Au nanocrystals with a concentration of 20 mg/mL onto a hand-cut silicon wafer with a size of approximately 7 mm × 7 mm. GISAXS data were recorded with *in situ* heating of the sample using an aluminum heating stage designed to minimizing the sample height variation due to the thermal
45 expansion of stage. Fit2D software (version: 12_077_i686_WXP) was used to process and integrate the GISAXS patterns and the GISAXS diffraction spots were indexed using the procedures described in Ref 37.

2.4 Differential Scanning Calorimetry (DSC) and Transmission Electron Microscopy (TEM)

DSC was conducted on a Mettler-Toledo DSC1. Samples were scanned in a 75 μL
5 aluminum crucible under N_2 atmosphere from 25°C to 70°C with a heating/cooling
rate of 5°C/min. TEM was performed on a FEI Tecnai Biotwin TEM operated at 80
kV accelerating voltage. Nanocrystals were drop cast onto a 200 mesh carbon-coated
copper grids for imaging (Electron Microsopy Science).

3 Results and Discussion

10 The average diameter and size distribution of the octadecanethiol-capped Au
nanocrystals were determined by SAXS measurements of nanocrystals dispersed in
toluene. Figure 1b shows SAXS data fit to calculations of the scattering intensity
$I(q)$, expected from a collection of non-interacting spherical particles:[36]

$$I(q) \propto \int_0^\infty N(R)P(qR)R^6 \, dR \quad . \tag{1}$$

15 The number distribution $N(R)$, of the nanocrystals of radius R, is assumed to be
Gaussian,

$$N(R) = \frac{1}{\sigma\sqrt{2\pi}} \exp\left[\frac{-(R - \overline{R})^2}{2\sigma^2} \right] \quad , \tag{2}$$

with mean radius $\overline{R}$, and standard deviation of σ. The shape factor $P(qR)$, for
spherical nanocrystals is

20
$$P(qR) = \left[3\frac{\sin(qR) - qR\cos(qR)}{(qR)^3} \right]^2 \quad , \tag{3}$$

The scattering wave vector is $q = (4\pi/\lambda)\sin(\theta/2)$, where λ is the X-ray wavelength
and θ is the scattering angle. Fitting Eqns (1)-(3) to the data in Fig. 1b yields an
average diameter for the nanocrystals of 1.66 ± 0.30 nm (18.3% polydispersity).
This size was verified by taking TEM images of the sample (See Supporting
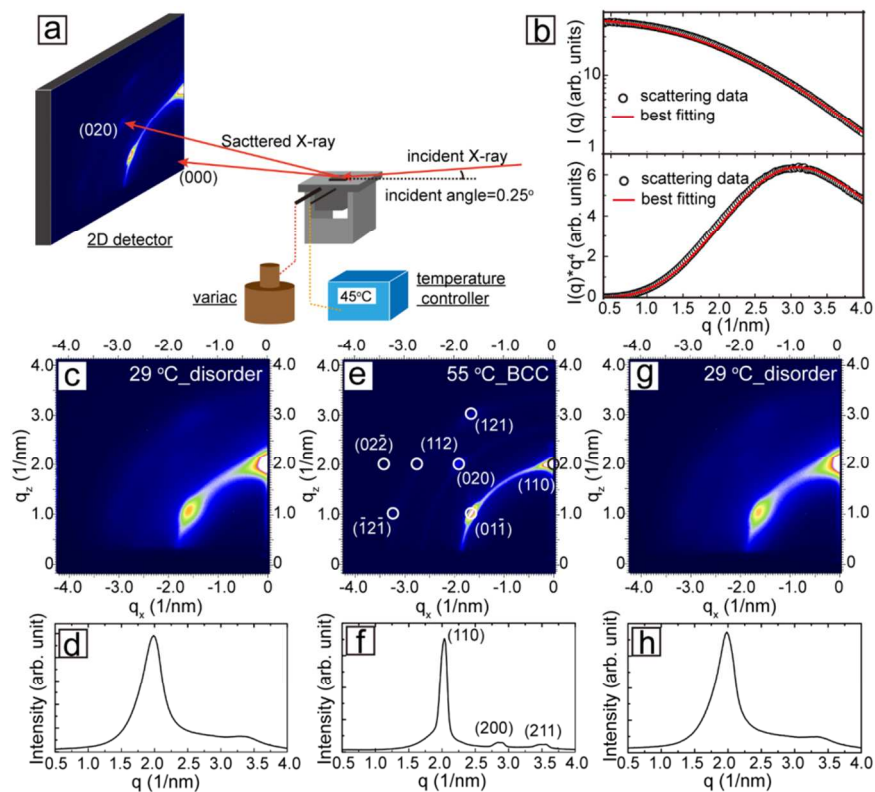25 Information).

Fig. 1 (a) Illustration of the GISAXS experiment setup with *in situ* heating capability. (b) SAXS data obtained from octadecanethiol-capped Au nanocrystals dispersed in toluene. A plot of Log($I(q)$) vs. q and a Porod plot are both shown with black circles as the data points and the red curves representing the best fit of Eqns
5 (1)-(3) to the data. GISAXS data are shown for assemblies of these nanocrystals at (c) at 29°C, (e) after heating to 55°C and then (g) cooling back to 29°C. Radial integrations of the patterns in (c), (e) and (g) are shown in (d), (f) and (h), respectively. The GISAXS pattern in (e) and its radial integration in (f) are indexed to a bcc superlattice with a lattice constant of $a_{bcc,SL} = 4.4$ nm .

10

Assemblies of octadecanethiol-capped Au nanocrystals were formed by drop-casting and were then examined by GISAXS using an experimental setup with *in situ* heating as illustrated in Figure 1a. GISAXS provides a powerful tool for determining the structure of nanocrystal films.[38,39] The 2D GISAXS pattern (Fig.
15 1c) of the assembly exhibits a couple of very weak diffraction spots that index to a body-centered cubic (bcc) superlattice.[40] The extent of order, however, is very limited. For instance, the radial integration of the GISAXS pattern shown in Fig. 1d is consistent with an amorphous structure, having a ratio of q values for the first two diffraction peaks of $q_2/q_1 = 1.67$.[41-43] The limited range of order in the assembly
20 reflects the relatively broad size distribution of the particles (>18% polydispersity).

Upon heating however, the superlattice order increased significantly. Figure 1e shows a GISAXS pattern obtained from the assembly from Fig. 1c heated to 55°C. The diffuse spots observed at room temperature are significantly sharper and more

intense, and additional diffraction spots have appeared. As shown in Fig. 1e, the 2D diffraction pattern indexes to a bcc superlattice oriented with its $(110)_{SL}$ planes on the substrate with a lattice constant of $a_{bcc,SL} = 4.4\,nm$. Diffraction peak indexing is also shown in Fig. 1f for the radial integration of the 2D data. A comparison of the radially-integrated data at 29°C and 55°C reveals quite clearly that the nanocrystal assembly has changed from being largely disordered to an bcc superlattice with relatively long range order.

When the assembly was returned to room temperature, the long-range superlattice order was again lost, as the scattering patterns in Figs 1g and 1h show. The 2D GISAXS pattern and its radial integration in Figs 1g and 1h are similar to those of the initial assembly in Figs. 1c and 1d.

When the assembly was heated again to 55°C, it reordered. The disorder-to-order and disorder-to-order transitions were reversible for many heating and cooling cycles. Figure 2 shows radially integrated GISAXS data obtained from five heating and cooling cycles, showing the reversibility of the transitions. A movie showing the evolution of the 2D GISAXS patterns obtained from an assembly being heated and cooled is also provided in Supporting Information.
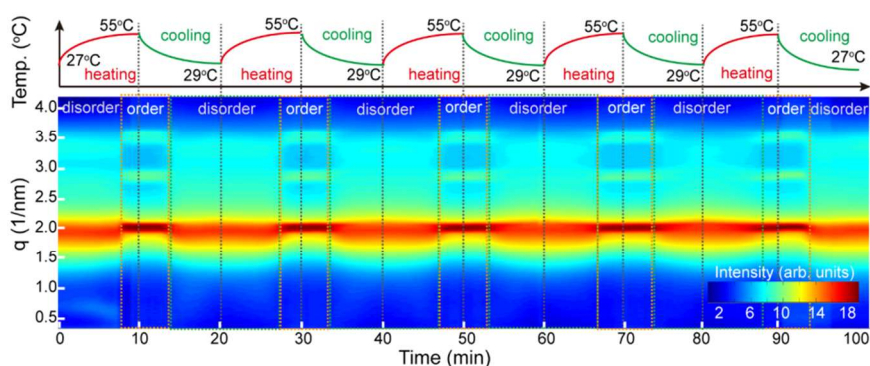

Fig. 2 Top: A plot of the temperature of the octadecanethiol-capped Au nanocrystal assembly vs. time. Bottom: Contour plot of scattering intensity $I(q)$ vs. time. The GISAXS patterns were recorded with each 1°C increase in temperature. Inset: Intensity scale in which red indicates high scattering intensity with blue indicates low intensity.

The disorder-to-order and order-to-disorder transition temperatures were estimated using the Hansen-Verlet criterion for freezing, which is an empirical rule suggesting that the first peak in the structure factor $S(q)$, is approximately 2.85 when crystallization occurs.[44] Figure 3a shows plots of $S(q)$ at various temperatures. The first peak maxima for $S(q)$ increased from 1.5 to 7 during heating and returned to 1.7 after cooling back near room temperature. Figure 3b shows the disorder-to-order (upon heating) and order-to-disorder (upon cooling) transition temperatures determined using the Hansen-Verlet criterion. The heating-induced disorder-to-order transition occurred at temperatures ranging between 45°C and 50°C, shifting slightly in temperature with each heating and cooling cycle. The order-to-disorder transitions occurred at slightly lower temperatures ranging from 35°C to 40°C.
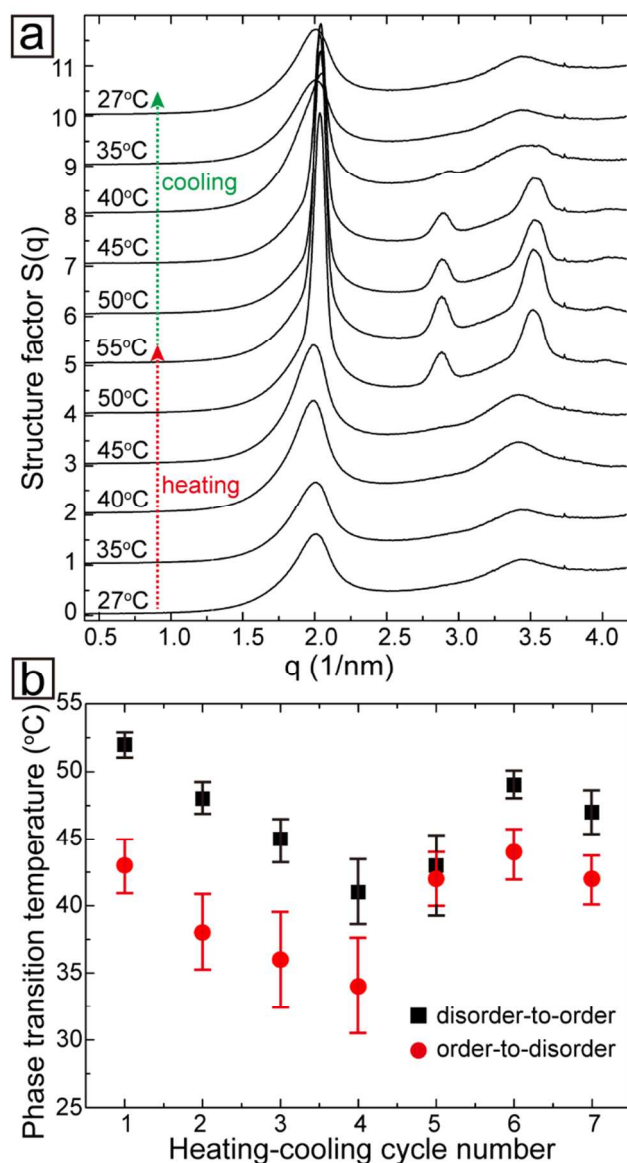
Fig. 3 (a) $S(q)$ of assemblies of octadecanethiol-capped Au nanocrystals calculated from radially-integrated GISAXS patterns by normalizing the diffraction data with the scattering profiles obtained from the solution SAXS measurements.[45] (See
5 Supporting Information for details) (b) Disorder-to-order and order-to-disorder transition temperatures determined using the Hansen-Verlet criterion for freezing plotted against heating-cooling cycle number.

The thermal behavior of the nanocrystal assemblies was also examined by DSC.
10 As shown in Fig 4., an endotherm is observed during sample heating at $56^{\circ}C$ and an

exotherm during sample cooling at 49°C. These temperatures are close to the disorder-order and order-disorder transitions determined from the diffraction data using the Hansen-Verlet criterion (Fig. 3b). The transition temperatures and the endotherm and exotherm temperatures measured by DSC are close to the melting and solidification temperatures of octadecanethiol.[46] Therefore, it appears that melting and solidification of the capping ligands is related to the ordering transition observed for the octadecanethiol-capped nanocrystals.
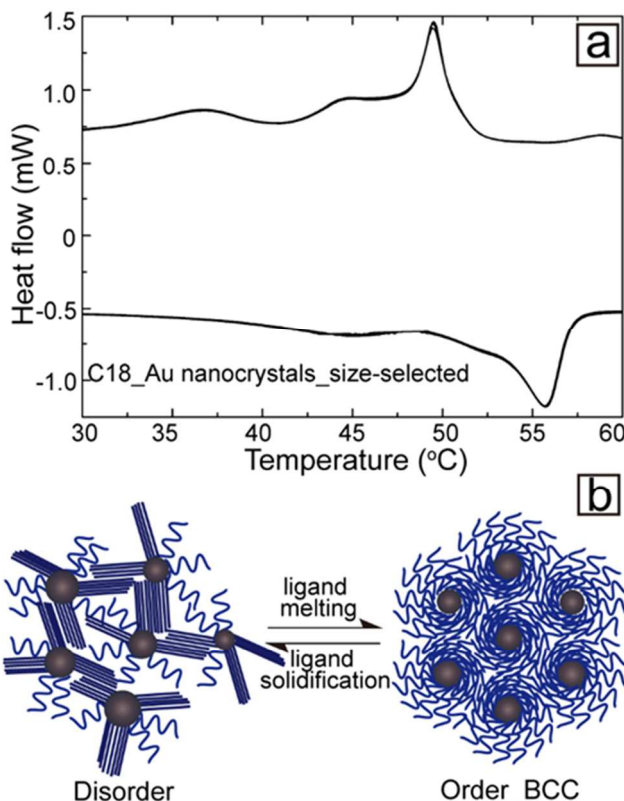

Fig. 4 (a) DSC of size-selected octadecanethiol-capped Au nanocrystals with average diameter of 1.66 ± 0.30 nm (18.3% polydispersity). Multiple overlapping scans confirm that the thermal transitions are reversible. (b) Illustration of how ligand melting and solidification can influence superlattice order.

Geyer, Born and Kraus,[23] reported related phenomena in which aggregates of alkanethiol-capped Au nanocrystals exhibited ordered packing when drop-cast onto TEM grids at temperatures above the ligand melting point, and disordered packing when drop-cast at lower temperatures. They proposed that ligands are solid-like, below their melting point, friction or "stickiness" between assembling particles occurs that inhibits order; whereas, liquid-like ligands provide the necessary mobility to obtain close-packed, ordered structures. Our situation is different, as the nanocrystals are assembled prior to heating (and cooling) and the dynamics of the

assembly process are not relevant. In our case, melting or solidification of the ligands appears to influence the uniformity of the interparticle interactions. Below the melting point of octadecanethiol, the ligands pack into ordered bundles, as illustrated in Fig. 4b.[25,46] Above the melting temperature of the ligands, the bundles are disrupted and the interparticle interactions become more uniform, again shown in Fig. 4b. This melted-ligand layer compensates for the Au core polydispersity and enables the nanocrystals to settle into a structure with ordered packing. An analysis of the effective nanocrystal size distribution that includes the ligand shell shows how this is possible. Polydispersities larger than 10% frustrate ordered packing of hard spheres.[47] And ligand-capped nanocrystals are slightly more tolerant to size non-uniformity because of the deformable capping ligands that can fill space and voids in the superlattice as necessary,[9] but polydispersities above about 12% still typically frustrate ordered packing.[48] In the case of these very small Au nanocrystals (1.66 nm diameter), the relatively long C_{18} capping ligands occupy an extremely large fraction of the superlattice volume: 94.4% (See Supporting Information). Considering the excluded volume of the ligands and the Au core diameter of 1.66 nm, the effective diameter of the nanocrystals—considering a ligand shell with uniform thickness and density—is 4.34 nm. The standard deviation in particle diameter due to the Au cores is ±0.30 nm, making the effective polydispersity of the sample only ±6.9%, which is well within the limits required for ordered packing.

We also found that there is a limit to how much the ligands can overcome polydispersity and enable ordering in the superlattice. Assemblies were made with octadecanethiol-capped Au nanocrystals that were not size-selected, having a core size of 1.75 ± 0.35 nm, corresponding to 20% polydispersity. Figures 5b and 5c show GISAXS patterns obtained from the assemblies at 29°C and 70°C. There is no evidence of superlattice order in either diffraction pattern. Figure 5a shows DSC data from these assemblies. The endotherm and exotherm signatures of octadecanethiol melting and solidification are still observed, but the nanocrystals did not order when heated above the octadecanethiol melting point.
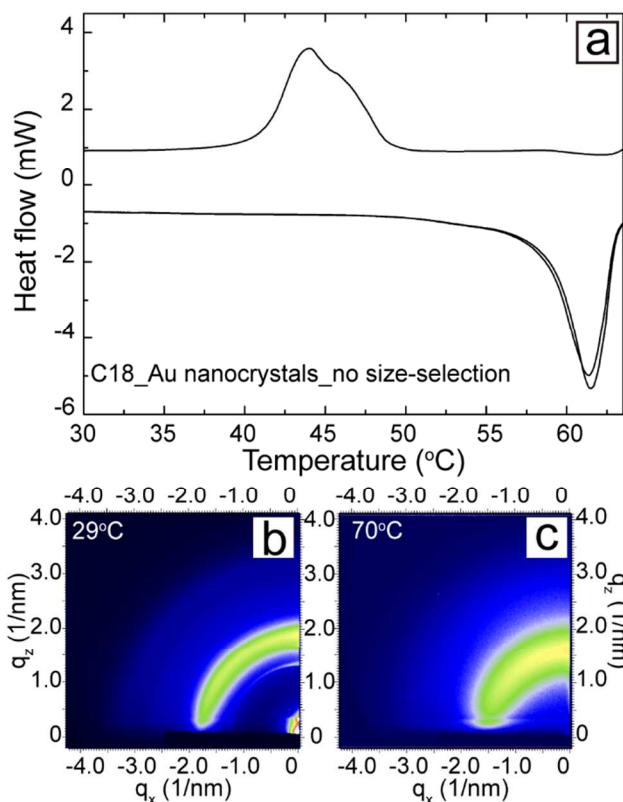
Fig. 5 (a) DSC of octadecanethiol-capped Au nanocrystals that were not size-selected (average diameter 1.75 ± 0.35 nm (20% polydispersity); and GISAXS patterns of an assembly of these nanocrystals (b) near room temperature, and (c) at 5 70°C. Neither pattern exhibits any evidence of long range superlattice order.

4 Conclusions

Assemblies of very small, 1.66 nm diameter, octadecanethiol-capped Au nanocrystals with a reasonably polydisperse size distribution (σ=18.3%) undergo an 10 ordering transition when heated. At room temperature, the assemblies are predominantly disordered, with only a slight evidence of short-range bcc order in the 2D GISAXS pattern. Once heated above 45-55°C, the nanocrystals order into a well-defined bcc superlattice. Qualitatively, this heat-induced disorder-to-order transition is similar to inverse melting, in which the crystalline state occurs at higher 15 temperature than the amorphous or liquid state.[34] DSC also showed an endotherm and exotherm associated with the disorder-to-order transition upon heating and the order-to-disorder structural transition upon cooling, as would be expected for an inverse melting transition.[31,49] These thermal features are also related to the melting and solidification of the octadecanethiol capping ligands. It appears that the capping 20 ligands compensate for the Au core polydispersity when heated above the melting

point of octadecanethiol.

This is the first *reversible* structural transition to be observed in a heated nanocrystal superlattice. The relatively mild transition temperature does not destroy the integrity of the nanocrystals. In all cases to date in which structure transitions in alkanethiol-capped Au nanocrystals have been observed with heating, the transitions have been irreversible due to ligand desorption and resulting changes in nanocrystal size.[26,50-57] This study provides new motivation to seek reversible structure transitions in nanocrystal superlattices, either through changes in temperature, pressure, or solvent vapor annealing and to seek systems with more robust ligand bonding, like alkyl-capped silicon nanocrystals for example.[48] More robust nanocrystals should provide even more interesting model systems to study superlattice structure transitions—especially those that are reversible—perhaps with the possibility of finally observing a true melting transition in a nanocrystal superlattice.

Acknowledgements

References

† Electronic Supplementary Information (ESI) available: Movie of GISAXS pattern evoluation with changes in temperature that shows the disorder-to-order and order-to-disorder transitions. TGA of size-selected octadecanethiol-capped Au nanocrystals, solution SAXS of octadecanethiol-capped Au nanocrystals prior to size-selection, structure factor calculations, TEM images of Au nanocrystals. This material is available free of charge via the internet at XXX.

1. M. Brust, M. Walker, D. Bethell, D. J. Schiffrin, R. Whyman, *Chem. Commun.*, 1994, 801-802.
2. A. E. Saunders, M. B. Sigman, B. A. Korgel, *J. Phys. Chem. B*, 2004, **108**, 193-199.
3. R. L. Whetten, M. N. Shafigullin, J. T. Khoury, T. G. Schaaff, I. Vezmar, M. M. Alvarez, A. Wilkinson, *Acct. Chem. Res.*, 1999, **32**, 397-406.
4. V. Santhanam, J. Liu, R. Agarwal; R. P. Andres, *Langmuir*, 2003, **19**, 7881-7887.
5. T. P. Bigioni, X.-M. Lin, T. T. Nguyen, E. I. Corwin, T. A. Witten, H. M. Jaeger, *Nature Mater.*, 2006, **5**, 265-270.
6. B. L. Prasad, C. M. Sorensen, K. J. Klabunde, *Chem. Soc. Rev.* , 2008, **37**, 1871-1883.
7. G. Ge, L. Brus, *J. Phys. Chem. B*, 2000, **104**, 9573-9575.
8. C. Stowell, B. A. Korgel, *Nano Lett.*, 2001, **1**, 595-600.
9. D. K. Smith, B. Goodfellow, D.-M. Smilgies, B. A. Korgel, *J. Am. Chem. Soc.*, 2009, **131**, 3281-3290.
10. P. C. Ohara, J. R. Heath, W. M. Gelbart, *Angew. Chem. Intl. Ed.*, 1997, **36**, 1078-1080.
11. A. E. Saunders, P. S. Shah, M. B. Sigman, T. Hanrath, H. S. Hwang, K. T. Lim, K. P. Johnston, B. A. Korgel, *Nano Lett.*, 2004, **4**, 1943-1948.
12. X. M. Lin, H. M. Jaeger, C. M. Sorensen, K. J. Klabunde, *J. Phys. Chem. B*, 2001, **105**, 3353-3357; N. Goubet, M.-P. Pileni, *Nano Res.* 2014, **7**, 171-179.
13. E. Rabani, D. R. Reichman, P. L. Geissler, L. E. Brus, *Nature*, 2003, **426**, 271-274.
14. B. A. Korgel, D. Fitzmaurice, *Phys. Rev. Lett.* 1998, **80**, 3531-3534.
15. M. B. Sigman, A. E. Saunders, B. A. Korgel, *Langmuir*, 2004, **20**, 978-983.
16. P. N. Pusey, E. Zaccarelli, C. Valeriani, E. Sanz, W. C. K. Poon, M. E. Cates, *Phil. Trans. R. Soc. A*, 2009, **367**, 4993-5011.
17. P. N. Pusey, W. van Megen, *Nature*, 1986, **320**, 340-342.

18. S. Sastry, T. M. Truskett, P. G. Debenedetti, S. Torquato, F. H. Stillinger, *Molecular Phys.*, 1998, **95**, 289-297.

19. H. Löwen, T. Palberg, R. Simon, *Phys. Rev. Lett.*, 1993, **70**, 1557-1560.

20. S. Torquato, F. H. Stillinger, *Rev. Mod. Phys.*, 2010, **82**, 2633-2672.

21. L. V. Woodcock, *Nature*, 1997, **385**, 141-143.

22. M. I. Bodnarchuk, M. V. Kovalenko, W. Heiss, D. V. Talapin, *J. Am. Chem. Soc.*, 2010, **132**, 11967-11977.

23. T. Geyer, P. Born, T. Kraus, *Phys. Rev. Lett.*, 2012, **109**, 128302.

24. A. E. Saunders, B. A. Korgel, *J. Phys. Chem. B*, 2004, **108**, 16732-16738.

25. W. D. Luedtke, U. Landman, *J. Phys. Chem.*, 1996, **100**, 13323-13329.

26. B. W. Goodfellow, M. R. Rasch, C. M. Hessel, R. N. Patel, D.-M. Smilgies, B. A. Korgel, *Nano Lett.*, 2013,**13**, 5712-5714.

27. K. Bian, J. J. Choi, A. Kaushik, P. Clancy, D.-M. Smilgies, T. Hanrath, *ACS Nano*, 2011, **5**, 2815-2823.

28. B. W. Goodfellow, B. A. Korgel, *ACS Nano*, 2011, **5**, 2419-2424.

29. T. Hanrath, *J. Vac. Sci. Tech. A*, 2012, **30**, 030802.

30. E. R. Dobbs, *Helium three*, Oxford University Press, Oxford, 2002.

31. S. Rastogi, M. Newman, A. Keller, *J. Poly. Sci. B*, 1993, **31**, 125-139.

32. C. S. J. van Hooy-Corstjens, G. W. H. Höhne, S. Rastogi, S. *Macromolecules*, 2005, **38**, 1814-1821.

33. M. R. Feeney, P. G. Debenedetti, F. H. Stillinger, *J. Chem. Phys.*, 2003, **119**, 4582-4591.

34. F. H. Stillinger, P. G. Debenedetti, *Biophys. Chem.*, 2003, **105**, 211-220.

35. M. R. Rasch, E. Rossinyol, J. L. Hueso, B. W. Goodfellow, J. Arbiol, B. A. Korgel, *Nano Lett.*, 2010, **10**, 3733-3739.

36. B. A. Korgel, S. Fullam, S. Connolly, D. Fitzmaurice, *J. Phys. Chem. B*, 1998, **102**, 8379-8388.

37. D.-M. Smilgies, D. R. Blasini, *J. Appl. Cryst.*, 2007, **40**, 716-718.

38. A. T. Heitsch, R. N. Patel, B. W. Goodfellow, D.-M. Smilgies, B. A. Korgel, *J. Phys. Chem. C*, 2010, **114**, 14427-14432.

39. D.-M. Smilgies, A. T. Heitsch, B. A. Korgel, *J. Phys. Chem. B*, 2012, **116**, 6017-6026.

40. B. W. Goodfellow, R. N. Patel, M. G. Panthani, D.-M. Smilgies, B. A. Korgel, *J. Phys. Chem. C*, 2011, **115**, 6397-6404.

41. H. W. Sheng, H. Z. Liu, Y. Q. Cheng, J. Wen, P. L. Lee, W. K. Luo, S. D. Shastri, E. Ma, *Nature Mater.*, 2007, **6**, 192-197.

42. J. T. Harris, J. L. Hueso, B. A. Korgel, *Chem. Mater.*, 2010, **22**, 6378-6383.

43. L. E. Pell, A. D. Schricker, F. V. Mikulec, B. A. Korgel, *Langmuir*, 2004, **20**, 6546-6548.

44. J.-P. Hansen, L. Verlet, *Phys. Rev.*, 1969, **184**, 151-161.

45. A. E. Saunders, P. S. Shah, E. J. Park, K. T. Lim, K. P. Johnston, B. A. Korgel, *J. Phys. Chem. B*, 2004, **108**, 15969-15975.

46. A. Badia, S. Singh, L. Demers, L. Cuccia, G. R. Brown, R. B. Lennox, *Chem. Eur. J.*, 1996, **2**, 359-363.

47. S.-E. Phan, W. B. Russel, J. Zhu, P. M. Chaikin, *J. Chem. Phys.*, 1998, **108**, 9789-9795.

48. Y. Yu, C. A. Bosoy, C. M. Hessel, D.-M. Smilgies, B. A. Korgel, *ChemPhysChem*, 2013, **14**, 84-87.

49. S. Rastogi, G. W. H. Höhne, A. Keller, *Macromolecules*, 1999, **32**, 8897-8909.

50. B. A. Korgel, N. Zaccheroni, D. Fitzmaurice, *J. Am. Chem. Soc.*, 1999, **121**, 3533-3534.

51. Y. Yu, C. A. Bosoy, D.-M. Smilgies, B. A. Korgel, B. *J. Phys. Chem. Lett.*, 2013, **4**, 3677-3682.

52. B. A. Korgel, *Phys. Rev. Lett.*, 2001, **86**, 127-130.

53. B. W. Goodfellow, R. N. Patel, M. G. Panthani, D.-M. Smilgies, B. A. Korgel, *J. Phys. Chem. C*, 2011, **115**, 6397-6404.

54. A. Courty, A.-I. Henry, N. Goubet, M.-P. Pileni, *Nature Mater.*, 2007, **6**, 900-907.

55. B. Ingham, T. H. Lim, C. J. Dotzler, A. Henning, M. F. Toney, R. D. Tilley, *Chem. Mater.*, 2011, **23**, 3312-3317.

56. B. Lee, P. Podsiadlo, S. Rupich, D. V. Talapin, T. Rajh, E. V. Shevchenko, *J. Am. Chem. Soc.*, 2009, **131**, 16386-16388.

57. A. V. Ellis, J. D'Arcy-Gall, K. Vijayamohanan, R. Goswami, P. G. Ganesan, C. Ryu, G. Ramanath, *Themochimica Acta*, 2005, **426**, 207-212.